Shuodao Wang
Department of Mechanical Engineering,
Northwestern University,
Evanston, IL 60208

Ming Li
State Key Laboratory of Structural
Analysis for Industrial Equipment,
Dalian University of Technology,
Dalian 116024, P. R. C.;
Department of Civil and Environmental Engineering,
Northwestern University,
Evanston, IL 60208

Jian Wu
Department of Engineering Mechanics,
Tsinghua University,
Beijing 100084, P. R. C.

Dae-Hyeong Kim
School of Chemical and Biological Engineering,
Seoul National University,
Seoul, 151-744, Korea

Nanshu Lu
Department of Aerospace Engineering and
Engineering Mechanics,
University of Texas at Austin,
Austin, TX 78705

Yewang Su
Department of Civil and Environmental Engineering,
Northwestern University,
Evanston, IL 60208

Zhan Kang
State Key Laboratory of Structural
Analysis for Industrial Equipment,
Dalian University of Technology,
Dalian 116024, P. R. C.

Yonggang Huang[1]
Department of Mechanical Engineering,
Northwestern University,
Evanston, IL 60208;
Department of Civil and
Environmental Engineering,
Northwestern University,
Evanston, IL 60208
e-mail: y-huang@northwestern.edu

John A. Rogers[1]
Department of Materials Science and Engineering,
Beckman Institute for Advanced
Science and Technology,
and Frederick Seitz Materials Research Laboratory,
University of Illinois at Urbana-Champaign,
Urbana, IL 61801
e-mail: jrogers@uiuc.edu

Mechanics of Epidermal Electronics

Epidermal electronic system (EES) is a class of integrated electronic systems that are ultrathin, soft, and lightweight, such that it could be mounted to the epidermis based on van der Waals interactions alone, yet provides robust, intimate contact to the skin. Recent advances on this technology will enable many medical applications such as to monitor brain or heart activities, to monitor premature babies, to enhance the control of prosthetics, or to realize human-machine interface. In particular, the contact between EES and the skin is key to high-performance functioning of the above applications and is studied in this paper. The mechanics concepts that lead to successful designs of EES are also discussed. The results, validated by finite element analysis and experimental observations, provide simple, analytical guidelines for design and optimization of EES with various possible functionalities. [DOI: 10.1115/1.4005963]
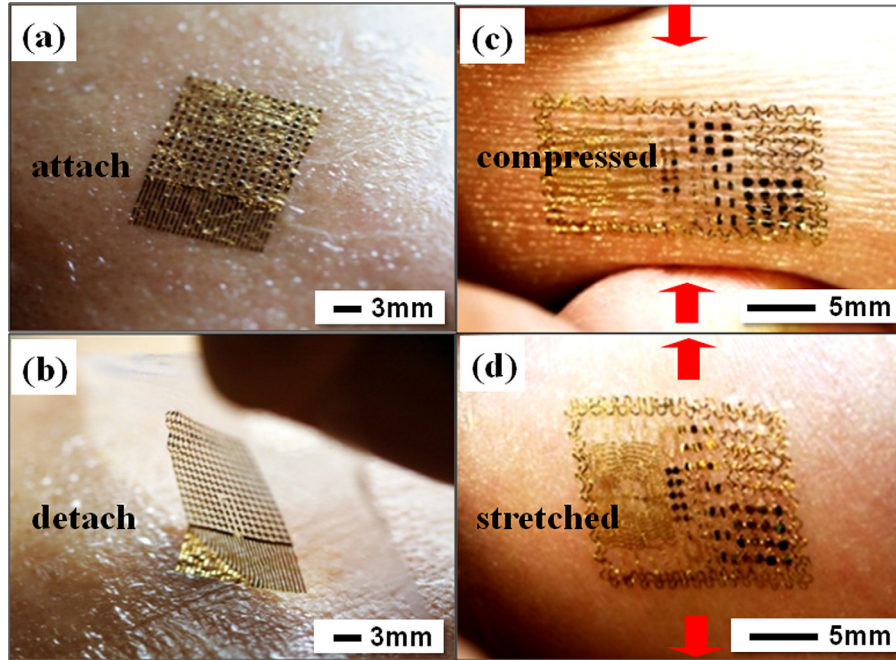
Keywords: work of adhesion, interfacial contact, epidermis, electronics

1 Introduction

Physiological measurements that exploit interfaces to the skin have been studied for over 80 years [1–3], but these conventional, wafer-based approaches are still poorly suited for practical applications outside of research labs due to difficulties in achieving

Fig. 1 (*a*) Image of a multifunctional, "skin-like" electronic system mounted to the skin on the forehead, which is used to monitor brain activity. (*b*) The integrated EES can be easily peeled away from the skin. (*c*) EES on skin remains in intimate contact with the skin when compressed. (*d*) EES on skin remains in intimate contact with the skin when stretched.

robust electrical contacts with the skin and in achieving portable integrated systems with small size, light weight, and biocompatible shapes [4–7]. Kim et al. [8] recently proposed a different technology, in which the electronic circuits, sensors, wireless power units, and communication components are integrated into ultrathin, low modulus, lightweight, stretchable membranes (Figs. 1(*a*) and 1(*b*)) that could be mounted onto the skin by van der Waals interactions alone in a manner that does not irritate the skin during prolong use. The epidermal electronic system is almost mechanically unnoticeable to the carrier, and could retain conformal contact with the skin under compression/tension (Figs. 1(*c*) and 1(*d*)). It will have many important medical applications such as to monitor brain activities, heart activities, or premature babies, to enhance the control of prosthetics, and to realize human-machine interface.

Physical coupling of electrodes to the surface of the skin is one of the most important features for many uses of EES and is studied via a simple, analytical mechanics model in this paper. It accounts for the macroscopic properties in Sec. 2 and microscopic morphology of the skin in Sec. 3. The effect of EES thickness and size and the contact pressure between EES and the skin is discussed in Sec. 4. Results are validated with finite element analysis and agree very well with experimental observations on two types of EES designs: (1) the filamentary serpentine (FS) EES (Fig. 2(*a*)) where ultrathin active devices (0.5 μm thick) adopt FS layouts and continuously integrate with narrow FS interconnects (100 μm wide), and (2) island-plus-serpentine (IPS) EES (Fig. 2(*c*)) where active device islands ($\sim$3.1 μm thick, squares of 500×500 μm^2) are integrated with similar FS interconnects.

2 Macroscopic Properties of the EES

The top-view and cross-section layouts of the FS-EES and IPS-EES are shown in Fig. 2. The FS-EES (Figs. 2(*a*) and 2(*b*)) consists of a backing layer of silicone (thickness $h_{\text{silicone}} = 30$ μm) and narrow FS strips (width 100 μm) made of polyimide (PI, thickness 0.3 μm) and gold (thickness 0.2 μm). The IPS-EES (Figs. 2(*c*) and 2(*d*)) consists the same backing layer and electrode

islands (thicknesses: PI 1.2 μm, gold 0.2 μm, PI 1.2 μm, gold 0.5 μm) interconnected with FS bridges.

The adhesion between the EES and the skin is determined by both the work of adhesion and the contact area. For the EES/skin interface, the contact between device strips/island (the gold layer in Figs. 2(*b*) and 2(*d*)) and skin is characterized by its work of adhesion $\gamma_{\text{device/skin}}$, while that for the contact between silicone and skin is $\gamma_{\text{silicone/skin}}$. The effective work of adhesion between EES and skin is then averaged as $\gamma = \alpha\gamma_{\text{device/skin}} + (1 - \alpha)\gamma_{\text{silicone/skin}}$, where α is the area fraction of devices. Since adhesion between the device (gold layer) and the skin is very weak (~ 0), the effective work of adhesion is simplified to

$$\gamma \approx (1 - \alpha)\gamma_{\text{silicone/skin}} \tag{1}$$

For the experimental value of $\gamma_{\text{silicone/skin}} = 0.2$ N/m measured by rod-rolling test [9], Eq. (1) gives $\gamma \approx 0.16$ N/m for the FS-EES ($\alpha \approx 22.5\%$ in Fig. 2(*a*) [8]) and $\gamma \approx 0.14$ N/m for the IPS-EES ($\alpha \approx 30.9\%$ in Fig. 2(*c*) [8]).

For narrow FS strips distributed over the entire surface of FS-EES, the effective bending stiffness of EES is averaged similarly as
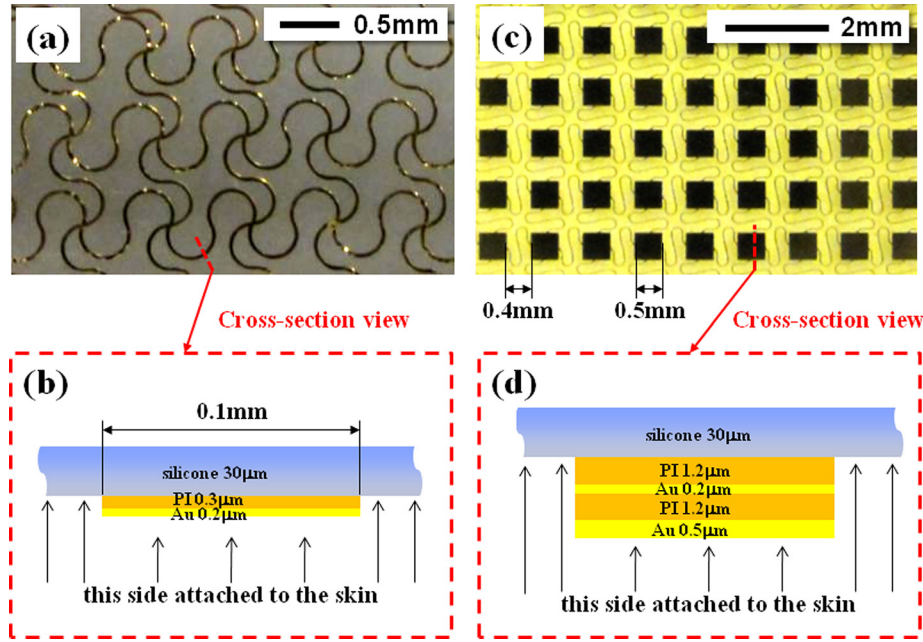
$$\overline{EI}_{\text{EES}} = \alpha\overline{EI}_{\text{device}} + (1 - \alpha)\overline{EI}_{\text{silicone}} \tag{2}$$

where $\overline{EI}_{\text{silicone}} = \overline{E}_{\text{silicone}}h_{\text{silicone}}^3/12$ is the bending stiffness of silicone ($\overline{E}_{\text{silicone}} = 65$ kPa is the plane-strain modulus of silicone). The bending stiffness for silicone with device is

$$\overline{EI}_{\text{device}} = \sum_{i=1}^{N} \overline{E}_i h_i \left[\left(b - \sum_{j=1}^{i} h_j \right)^2 + \left(b - \sum_{j=1}^{i} h_j \right) h_i + \frac{1}{3} h_i^2 \right] \tag{3}$$

with

$$b = \sum_{i=1}^{N} \overline{E}_i h_i \left(\sum_{j=1}^{i} h_j - \frac{1}{2} h_i \right) \bigg/ \sum_{i=1}^{N} \overline{E}_i h_i \tag{4}$$

Fig. 2 (*a*) Top view of the FS-EES layouts. (*b*) Cross-section view of the FS-EES layouts. (*c*) Top view of the IPS-EES layouts. (*d*) Cross-section view of the IPS-EES layouts.

where $N = 3$ is the number of layers, $\overline{E}_1 = \overline{E}_{\text{silicone}}$, $h_1 = h_{\text{silicone}}$, $\overline{E}_2 = \overline{E}_{\text{polyimide}} = 2.8$ GPa and $h_2 = 0.3$ μm are the plane-strain modulus and thickness for polyimide, and $\overline{E}_3 = \overline{E}_{\text{Au}} = 97$ GPa and $h_3 = 0.2$ μm for gold. For $\alpha \approx 22.5\%$ from Fig. 2(*a*), Eqs. (2)–(4) gives the effective bending stiffness 0.27×10^{-9} N-m, which agrees reasonably well with 0.30×10^{-9} N-m obtained by finite element analysis.

For IPS-EES, the isolated device islands (total thickness of 3.1 μm) are much thicker than FS-EES (thickness 0.5 μm) and also much larger (500×500 μm^2 pads for IPS-EES as compared to strips of 100 μm wide for FS-EES), such that the contact between the EES and the skin is mainly determined by the bending stiffness of the island devices $\overline{EI}_{\text{island}}$. For the IPS-EES in Figs. 2(*c*) and 2(*d*), the effective bending stiffness is given by Eqs. (3) and (4) as $\overline{EI}_{\text{EES}} = \overline{EI}_{\text{island}} = 4.6 \times 10^{-8}$ N-m, where $N = 5$, $\overline{E}_1 = \overline{E}_{\text{silicone}}$, $\overline{E}_2 = \overline{E}_4 = \overline{E}_{\text{polyimide}}$, $\overline{E}_3 = \overline{E}_5 = \overline{E}_{\text{Au}}$, $h_1 = 30$ μm, $h_2 = h_4 = 1.2$ μm, $h_3 = 0.2$ μm, and $h_5 = 0.5$ μm.

The FS-EES has an effective bending stiffness $\overline{EI}_{\text{EES}}$ given in Eq. (2) because FS are uniformly dispersed in the device. For FS-EES subject to a bending moment M, the bending curvature is approximately uniform and equals to $M/\overline{EI}_{\text{EES}}$. The IPS-EES, however, cannot be homogenized into an effective medium because the relatively large, thick device islands are discretely isolated. The local bending stiffness of the part with the device island is $\overline{EI}_{\text{island}} = 4.6 \times 10^{-8}$ N-m, which is ~ 300 times larger than the local bending stiffness of the part without the device island $\overline{EI}_{\text{spacing}} = \overline{E}_{\text{silicone}} h_{\text{silicone}}^3 / 12 = 1.5 \times 10^{-10}$ N-m. Therefore, the bending curvature $\kappa_{\text{spacing}} \sim 300 \kappa_{\text{island}}$, which is verified in the finite element analysis.

3 Contact Between EES and Skin

Microscopic morphology of the skin is accounted for in this section to study the contact between the EES and skin. The skin surface can be represented by a sinusoidal form $y(x) = h_{\text{rough}} \left[1 + \cos(2\pi x / \lambda_{\text{rough}}) \right] / 2$ with skin roughness amplitude h_{rough} and wavelength λ_{rough}. For non-conformal contact (Fig. 3, top) between the EES and skin, the former remains flat and the contact area is almost zero, which gives the total energy $\overline{U}_{\text{non-conformal}} = 0$.

For conformal contact (Fig. 3, bottom), both the EES and the skin deform to give their total displacement the same as the skin roughness $y(x)$. The displacements of EES and skin surface can be represented by
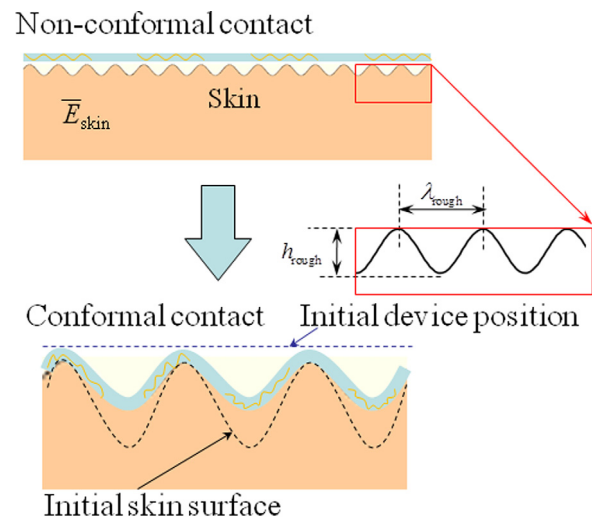
$$w(x) = \frac{h}{2}\left(1 + \cos\frac{2\pi x}{\lambda_{\text{rough}}}\right) \tag{5}$$

and

$$u_z(x) = y - w = \frac{h_{\text{rough}} - h}{2}\left(1 + \cos\frac{2\pi x}{\lambda_{\text{rough}}}\right) \tag{6}$$

respectively, where the maximum deflection h of EES is to be determined.

The total energy (per unit length along the wavelength direction) for conformal contact is $\overline{U}_{\text{conformal}} = \overline{U}_{\text{bending}} + \overline{U}_{\text{skin}} + \overline{U}_{\text{adhesion}}$. The total energy also consists of the localized

Fig. 3 Mechanics model analyzing the contact between EES and the skin, comparing the total energy of non-conformal contact state (top) and that of conformal contact state (bottom)

deformation energy near the device edges where the silicone and the skin deformed to overcome the device thickness and contact each other (Fig. 7). But the energy of this localized deformation $\overline{U}_{\text{local}}^{\text{deform}}$ is negligible compared to the bending energy ($\overline{U}_{\text{local}}^{\text{deform}}/\overline{U}_{\text{bending}} \sim 0.1\%$ for FS-EES and ~ 0.1 for IPS-EES, see Appendix for details) because the silicone and the skin are much softer than the device and the device thicknesses are much smaller than either the width of the devices or the thickness of silicone and skin. The bending energy of EES is

$$\overline{U}_{\text{bending}} = \frac{1}{\lambda_{\text{rough}}} \int_0^{\lambda_{\text{rough}}} \frac{\overline{EI}_{\text{EES}}(w'')^2}{2} dx = \frac{\pi^4 \overline{EI}_{\text{EES}} h^2}{\lambda_{\text{rough}}^4} \quad (7)$$

where $\overline{EI}_{\text{EES}}$ is the effective bending stiffness of EES given by Eq. (2). The skin is much thicker than the EES and, therefore, is modeled as a semi-infinite body subject to the surface displacement of Eq. (6). The normal stress on the top surface of the skin is obtained analytically as [10]

$$\sigma_z = \frac{\pi \overline{E}_{\text{skin}}(h_{\text{rough}} - h)}{2\lambda_{\text{rough}}} \cos \frac{2\pi x}{\lambda_{\text{rough}}} \quad (8)$$

and, therefore, the elastic energy of the skin is [10]

$$\overline{U}_{\text{skin}} = \frac{1}{\lambda_{\text{rough}}} \int_0^{\lambda_{\text{rough}}} \frac{\sigma_z u_z}{2} dx = \frac{\pi \overline{E}_{\text{skin}}(h_{\text{rough}} - h)^2}{16\lambda_{\text{rough}}} \quad (9)$$

The interfacial adhesion energy is the work of adhesion multiplied by the contact area, which gives

$$\overline{U}_{\text{adhesion}} = -\gamma \int_0^{\lambda_{\text{rough}}} \sqrt{1 + (w')^2} dx \approx -\gamma \left(1 + \frac{\pi^2 h^2}{4\lambda_{\text{rough}}^2}\right) \quad (10)$$

for the case of $\lambda_{\text{rough}} \sim 7 h_{\text{rough}}$ in experiments [8]. Minimization of the total energy then gives analytically the maximum deflection of EES as

$$h = \frac{\overline{E}_{\text{skin}} h_{\text{rough}}}{\dfrac{16\pi^3 \overline{EI}_{\text{EES}}}{\lambda_{\text{rough}}^3} + \overline{E}_{\text{skin}}} \quad (11)$$

For skin with $\overline{E}_{\text{skin}} \approx 130$ kPa, $\lambda_{\text{rough}} \approx 140$ μm [11] and average $h_{\text{rough}} \approx 55$ μm [12], and Eq. (11) gives the maximum deflection to be ~ 40 μm for FS-EES ($\overline{EI}_{\text{EES}} \approx 0.27 \times 10^{-9}$ N-m) and 0.85 μm for IPS-EES ($\overline{EI}_{\text{EES}} \approx 4.6 \times 10^{-8}$ N-m).

The total energy for conformal contact is then obtained as

$$\overline{U}_{\text{conformal}} = \overline{U}_{\text{bending}} + \overline{U}_{\text{skin}} + \overline{U}_{\text{adhesion}} = \frac{\pi^4 \overline{EI}_{\text{EES}} h_{\text{rough}}^2}{\lambda_{\text{rough}}^4 \left(\dfrac{16\pi^3 \overline{EI}_{\text{EES}}}{\overline{E}_{\text{skin}} \lambda_{\text{rough}}^3} + 1\right)}$$
$$- \frac{\pi^2 \gamma h_{\text{rough}}^2}{4\lambda_{\text{rough}}^2} \left[\frac{4\lambda_{\text{rough}}^2}{\pi^2 h_{\text{rough}}^2} + \frac{1}{\left(\dfrac{16\pi^3 \overline{EI}_{\text{EES}}}{\overline{E}_{\text{skin}} \lambda_{\text{rough}}^3} + 1\right)^2}\right] \quad (12)$$

Conformal contact requires $\overline{U}_{\text{conformal}} < \overline{U}_{\text{non-conformal}}$, which gives

$$\frac{4\pi^2 \overline{EI}_{\text{EES}}}{\gamma \lambda_{\text{rough}}^2} < \frac{4\lambda_{\text{rough}}^2}{h_{\text{rough}}^2 \pi^2} \left(\frac{16\pi^3 \overline{EI}_{\text{EES}}}{\overline{E}_{\text{skin}} \lambda_{\text{rough}}^3} + 1\right) + \frac{1}{\dfrac{16\pi^3 \overline{EI}_{\text{EES}}}{\overline{E}_{\text{skin}} \lambda_{\text{rough}}^3} + 1} \quad (13)$$
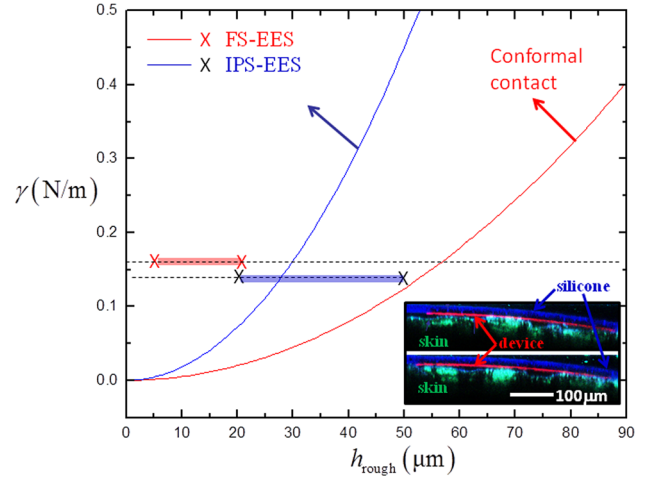
Fig. 4 Deformation map governing the conformal contact for FS-EES (curve on the right) and IPS-EES (curve on the left). The inset shows cross-section view of partial contact between IPS-EES and pig skin under confocal microscopy, with the silicone layer dyed to blue, the device to red and the skin to green. (Color figure available online.)

Since $\lambda_{\text{rough}} \sim 7 h_{\text{rough}}$ in experiments, the second term on the right hand side is negligible and Eq. (13) becomes

$$\frac{\pi \overline{E}_{\text{skin}} h_{\text{rough}}^2}{\gamma \lambda_{\text{rough}}} < 16 + \frac{\overline{E}_{\text{skin}} \lambda_{\text{rough}}^3}{\pi^3 \overline{EI}_{\text{EES}}} \quad (14)$$

The above scaling law involves two dimensionless combinations of EES and skin properties, $\overline{E}_{\text{skin}} h_{\text{rough}}^2 / (\gamma \lambda_{\text{rough}})$ and $\overline{E}_{\text{skin}} \lambda_{\text{rough}}^3 / \overline{EI}_{\text{EES}}$. It clearly shows that EES with low bending stiffness (thin, soft devices/backing layer), smooth and soft skin, and strong adhesion all promote conformal contact. For FS-EES (Fig. 2(a)), $\gamma \approx 0.16$ N/m and $\overline{EI}_{\text{EES}} \approx 0.27 \times 10^{-9}$ N-m (Sec. 2). The above criterion implies that EES can have conformal contact with skin when the skin roughness amplitude is smaller than ~ 56 μm (Fig. 4, curve on the right). This result is consistent with conformal contact observed in experiments where the FS-EES is mounted to pig skin with roughness amplitude ranging from $5 \sim 10$ μm [8] (range of roughness amplitude marked by the bar at $\gamma = 0.16$ in Fig. 4).

For the IPS-EES (Fig. 2(c)), the effective bending stiffness is $\overline{EI}_{\text{EES}} \approx 4.6 \times 10^{-8}$ N-m and the effective work of adhesion is $\gamma \approx 0.14$ N/m from Sec. 2. The criterion above implies that EES loses conformal contact once the skin roughness amplitude exceeds 27 μm (Fig. 4, curve on the left), which is consistent with partial contact observed in the confocal microscopy image (Fig. 4 inset) where the range of skin roughness is $20 \sim 50$ μm (marked by the bar at $\gamma = 0.14$ in Fig. 4).

4 Discussions: The Effect of Thickness and the "Wearability" of the EES

For FS-EES, the effect of device thickness is studied by changing thicknesses of all layers proportionally. Let h_{device} denote the total thickness of the device. Figure 5 shows that, for FS made of polyimide-gold as in experiments, the skin roughness for conformal contact decreases from ~ 56 μm to ~ 30 μm as the device thickness increases by 8 times. Therefore, thin devices promote conformal contact between EES and skin (so do soft, compliant devices).

The thickness and modulus of the device and the skin roughness also play important roles on the comfort, or wearability, of EES. The contact pressure at the EES-skin interface is obtained analytically from Eq. (8) and Eq. (11) as
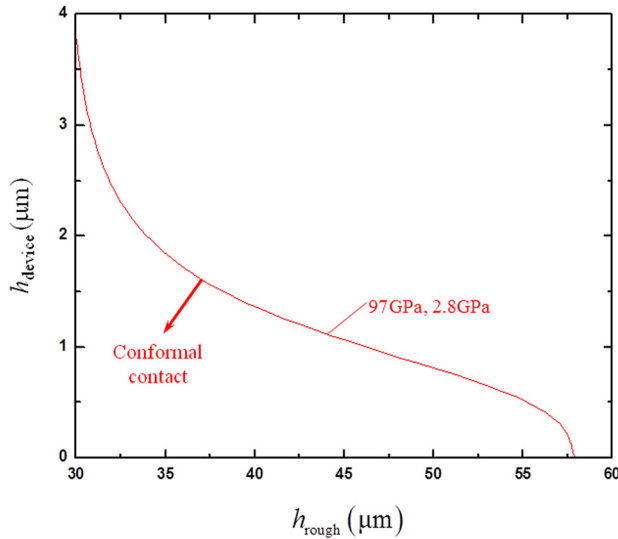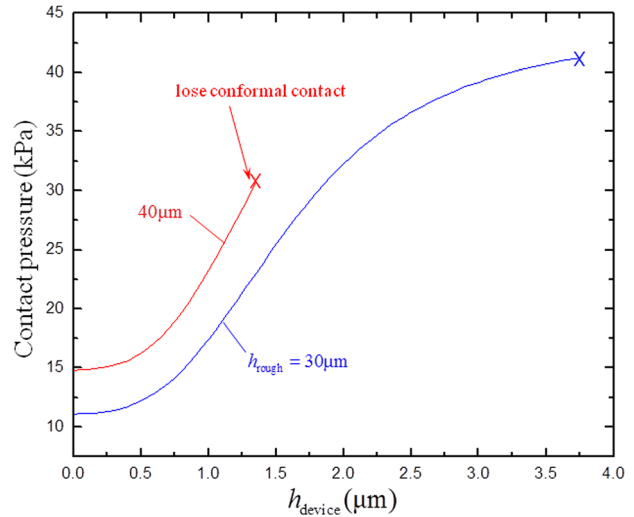
Fig. 5 Conformal contact requirement for FS-EES with devices of different thicknesses

Fig. 6 Contact pressure between an FS-EES and skin with different roughnesses

$$\sigma_{\text{contact}} = \frac{8\pi^4 \overline{E}_{\text{skin}} h_{\text{rough}}}{16\pi^3 \lambda_{\text{rough}} + \dfrac{\overline{E}_{\text{skin}} \lambda_{\text{rough}}^4}{\overline{EI}_{\text{EES}}}} \cos\frac{2\pi x}{\lambda_{\text{rough}}} \qquad (15)$$

Figure 6 (curve for 30 μm) shows the maximum contact pressure between FS-EES with various thicknesses and skin of average roughness ($h_{\text{rough}} = 30$ μm). For FS-EES with device thickness of 0.5 μm in experiments, the maximum contact pressure is only 12.5 kPa, which is below the human skin sensitivity ($\sim$20 kPa [13]) and, therefore, is mechanically unnoticeable and would not induce discomfort. Devices thicker than 1.2 μm give a contact pressure higher than 20 kPa, while devices thicker than 3.8 μm lose conformal contact to the skin. Rougher skin with $h_{\text{rough}} = 40$ μm (Fig. 6, curve for 40 μm) results in higher interfacial pressure, and the device thickness to lose conformal contact becomes much smaller ($\sim$1.5 μm). From Eq. (15), it is obvious that thinner, softer device gives smaller contact pressure and, thus, is more comfortable for the carrier.

5 Concluding Remarks

Simple, analytical mechanics concepts presented in this study lead to successful design of integrated high-performance, highly portable EES that offers robust, intimate contact with the surface of the skin. The scaling law governing the conformal contact between EES and the skin, the effects of device thickness, size and skin roughness, and the contact pressure on the surface of the skin are all studied in details. The results, validated by finite element analysis, agree well with experimental observations and are useful for future designs that exploit different functionality of EES.

Appendix

Since the device thickness h_{device} (0.50 μm for FS-EES and 3.1 μm for IPS-EES) is much smaller than that of the skin ($\sim$1 mm) and the silicone ($\sim$30 μm) and the device width w (100 μm for FS-EES and 500 μm for IPS-EES), the devices between the skin and silicone are analogous to inserting rigid wedges of uniform thickness h_{device} at the skin/silicone interface in a periodic pattern, leading to interfacial cracks and localized deformation near the crack tips, as shown in Fig. 7. The localized deformation energy *per unit length* is well studied by Huang et al. [14], and has the expression of
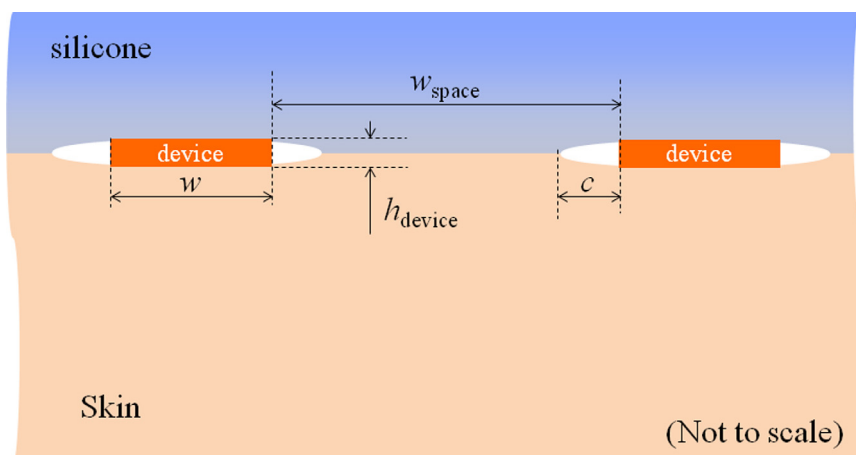
Fig. 7 Schematic cross-section view of EES at the interface between skin and silicone

$$\overline{U}_{\text{local}}^{\text{deform}} = \frac{\pi^2 \left(\overline{E}_{\text{skin}} + \overline{E}_{\text{silicone}}\right) h_{\text{device}}^2}{256 \left(w + w_{\text{space}}\right) \left(1 + \frac{w_{\text{space}} - 2c}{w + 2c}\right) \ln \left[\sec \left(\frac{\pi}{2} \frac{1}{1 + \frac{w_{\text{space}} - 2c}{w + 2c}}\right)\right]} \frac{K\left(\frac{w}{w + 2c}\right)}{K\left[\sqrt{1 - \frac{w^2}{(w + 2c)^2}}\right]} \tag{A1}$$

where w_{space} is the spacing between devices, c is the crack length (Fig. 7), and K is the complete elliptic integral of the first kind. The potential energy consists of the deformation energy in Eq. (A1) and the adhesive energy per unit length $\overline{U}_{\text{local}}^{\text{adhesive}} = 2\gamma c / \left(w + w_{\text{space}}\right)$. Minimizing the potential energy, $\partial\left(\overline{U}_{\text{local}}^{\text{deform}} + \overline{U}_{\text{local}}^{\text{adhesive}}\right)/\partial c = 0$ then gives numerically the crack length c, and therefore the deformation energy in Eq. (A1) could be determined. For skin with $\overline{E}_{\text{skin}} \approx 130$ kPa, $\lambda_{\text{rough}} \approx 140$ μm [11], average $h_{\text{rough}} \approx 55$ μm [12], and $w_{\text{space}} = 0.65$ mm, $\overline{EI}_{\text{EES}} \approx 0.27 \times 10^{-9}$ N-m for FS-EES, $w_{\text{space}} = 0.40$ mm, $\overline{EI}_{\text{EES}} \approx 4.6 \times 10^{-8}$ N-m for IPS-EES, the localized deformation energy from Eq. (A1) is very small compared to the bending energy from Eq. (7) ($\overline{U}_{\text{local}}^{\text{deform}} / \overline{U}_{\text{bending}} \sim 0.1\%$ for FS-EES and ~ 0.1 for IPS-EES) and therefore is negligible.

References

[1] Berger, H., 1929, "Uber das electrenkephalogramm des menchen," Arch. Psychiatr. Nervenkr, **87**, pp. 527–570.

[2] Fox, E. J., and Melzack, R., 1976, "Transcutaneous Electrical Stimulation and Acupuncture: Comparison of Treatment for Low-Back Pain," Pain, **2**(2), pp. 141–148.

[3] Hardyck, C. D., Petrinovich, L. F., and Ellsworth, D. W., 1966, "Feedback of Speech Muscle Activity During Silent Reading: Rapid Extinction," Science, **154**(3755), pp. 1467–1468.

[4] Webster, J. G., 2009, *Medical Instrumentation: Application and Design*, Wiley, Hoboken, NJ.

[5] Mannsfeld, S. C. B., Tee, B. C. K., Stoltenberg, R. M., Chen, C. V. H. H., Barman, S., Muir, B. V. O., Sokolov, A. N., Reese, C., and Bao, Z., 2010, "Highly Sensitive Flexible Pressure Sensors With Microstructured Rubber Dielectric Layers," Nat. Mater., **9**(10), pp. 859–864.

[6] Someya, T., Kato, Y., Sekitani, T., Iba, S., Noguchi, Y., Murase, Y., Kawaguchi, H., and Sakurai, T., 2005, "Conformable, Flexible, Large-Area Networks of Pressure and Thermal Sensors With Organic Transistor Active Matrixes," Proc. Natl. Acad. Sci. U.S.A., **102**(3), pp. 12321–12325.

[7] Takei, K., Takahashi, T., Ho, J. C., Ko, H., Gillies, A. G., Leu, P. W., Fearing, R. S., and Javey, A., 2010, "Nanowire Active-Matrix Circuitry for Low-Voltage Macroscale Artificial Skin," Nat. Mater., **9**(10), pp. 821–826.

[8] Kim, D.-H., Lu, N., Ma, R., Kim, Y.-S., Kim, R.-H., Wang, S., Wu, J., Won, S. M., Tao, H., Islam, A., Yu, K. J., Kim, T.-I., Chowdhury, R., Ying, M., Xu, L., Li, M., Chung, H.-J., Keum, H., McCormick, M., Liu, P., Zhang, Y.-W., Omenetto, F. G., Huang, Y., Coleman, T., and Rogers, J. A., 2011, "Epidermal Electronics," Science, **333**(6044), pp. 838–843.

[9] Meitl, M. A., Zhu, Z.-T., Kumar, V., Lee, K. J., Feng, X., Huang, Y. Y., Adesida, I., Nuzzo, R. G., and Rogers, J. A., 2006, "Transfer Printing by Kinetic Control of Adhesion to an Elastomeric Stamp," Nat. Mater., **5**(1), pp. 33–38.

[10] Jiang, H., Sun, Y., Rogers, J. A., and Huang, Y., 2008, "Post-Buckling Analysis for the Precisely Controlled Buckling of Thin Film Encapsulated by Elastomeric Substrates," Int. J. Solids Struct., **45**(7–8), pp. 2014–2023.

[11] Schwindt, D. A., Wilhelm, K. P., Miller, D. L., and Maibach, H. I., 1998, "Cumulative Irritation in Older and Younger Skin: A Comparison," Acta Derm. Venereol., **78**(4), pp. 279–283.

[12] Tchvialeva, L., Zeng, H., Markhvida, I., McLean, D. I., Lui, H., and Lee, T. K., 2010, "Skin Roughness Assessment," New Developments in Biomedical Engineering, D. Campolo, ed., InTech, http://www.intechopen.com/articles/show/title/skin-roughness-assessment.

[13] Kaneko, A., Asai, N., and Kanda, T., "The Influence of Age on Pressure Perception of Static and Moving Two-Point Discrimination in Normal Subjects," J. Hand Ther., **18**(4), pp. 421–425.

[14] Huang, Y. Y., Zhou, W., Hsia, K. J., Menard, E., Park, J.-U., Rogers, J. A., and Alleyne, A. G., 2005, "Stamp Collapse in Soft Lithography," Langmuir, **21**(17), pp. 8058–8068.